Chapter 4
Thermal Desorption Spectra of Samples Charged by Hydrogen in Electrolyte

Anastasia A. Chevrychkina, Vladimir A. Polyanskiy, and Evgenii A. Varshavchik

Abstract In the framework of the diffusion equation, we discuss the influence of hydrogen distribution in the sample on thermal desorption spectroscopy. We show that non-uniform hydrogen distribution after precharging may significantly affect the Choo-Lee plot. We demonstrate that taking into account influence of hydrogen distribution is important for understanding experimental results. Good comparison of experimental and modeling data is also shown.

Keywords Hydrogen diffusion · Choo-Lee plot · Thermal Desorption Spectra

4.1 Introduction

Absorbed hydrogen affects the mechanical behavior of metal. This is the reason that an analysis of hydrogen transport and the distribution of hydrogen atoms in metals is important in metallurgy. Hydrogen permeability through metal was discovered as early as 1864 [1], and the study of hydrogen permeability is still of interest for many engineering applications, including in the field of energy: hydrogen, nuclear, thermonuclear, and thermal energy. Hydrogen permeability of metals is investigated by many researchers [2–4]. Another problem associated with the interaction of hydrogen and metals is hydrogen embrittlement. Hydrogen embrittlement is responsible for

A. A. Chevrychkina (✉) · V. A. Polyanskiy
Institute for Problems in Mechanical Engineering RAS, V.O., Bolshoy pr., 61,
St. Petersburg 199178, Russia
e-mail: Anastasiia.Che@gmail.com

V. A. Polyanskiy
e-mail: vapol@mail.ru

E. A. Varshavchik
Peter the Great Saint-Petersburg Polytechnic University, Polytekhnicheskaya, 29.,
St. Petersburg 195259, Russia
e-mail: varshavchik.ea@edu.spbstu.ru

© The Author(s), under exclusive license to Springer Nature Switzerland AG 2021

V. A. Polyanskiy and A. K. Belyaev (eds.), *Advances in Hydrogen Embrittlement Study*,
Advanced Structured Materials 143, https://doi.org/10.1007/978-3-030-66948-5_4

premature and/or delayed rupture of materials and has become a concern in terms of the durability of materials. The hydrogen embrittlement phenomenon was first described by Johnson in 1875 [5]. Many papers are devoted to hydrogen embrittlement [6, 7].

It is assumed that the effect of hydrogen on the properties of metals is caused by absorbed hydrogen on traps such as dislocations, impurities, and internal interfaces, voids, micro-cracks, and other defects. Now the most developed approaches for the study of diffusion in solid are the approaches based on Fick's laws and statistical thermodynamics, which was proposed by Kirchheim in work [8]. The influence of traps is taken into account in both approaches.

McNabb and Foster [9] were the first to suggest separating flux of the lattice hydrogen concentration and the trapped hydrogen concentration in 1963.

$$\begin{cases} \dfrac{\partial C_L}{\partial t} + N_x \dfrac{\partial \theta_x}{\partial t} = D_L \dfrac{\partial^2 C_L}{\partial x^2}, \\ \dfrac{\partial \theta_x}{\partial t} = kC_L(1-\theta_x) - p\theta_x, \end{cases}$$

where C_L and D_L are hydrogen concentration and diffusivity in normal lattice, respectively; θ_x and N_x are occupancy and density of trap sites, respectively; k is the probability of hydrogen jumping from normal lattice site to trap site; and p is the probability of hydrogen releasing from trap site to normal lattice site.

Oriane showed the standard solutions of the diffusion equations with effective diffusion coefficient can be used to analyze experimental results in the case of assumption of local equilibrium for a restricted domain of degree of trap coverage in 1970 [10].

In 1979, Johnson brought a refinement on the limited capacity of traps, and proposed a clear dependence of the trap concentration on the lattice concentration [11]. Johnson model is the special case of the more general model McNabb and Foster.

Further development of the approach was made by Leblond and Dubois in 1983 [12]. They suggested introducing a new type of irreversible trap and analyzing the combined effects of reversible and irreversible traps. In 1989, the generalized model of hydrogen transport was developed by Turnbull which incorporated the combined effects of reversible and irreversible traps with varying degrees of occupancy [13]. Equations are described by

$$\begin{cases} \dfrac{\partial C}{\partial t} = D\dfrac{\partial^2 C}{\partial x^2} - N_r \dfrac{\partial \theta_r}{\partial t} - N_i \dfrac{\partial \theta_i}{\partial t}, \\ \dfrac{\partial \theta_r}{\partial t} = k_r C(1-\theta_r) - p\theta_r, \\ \dfrac{\partial \theta_i}{\partial t} = k_i C(1-\theta_i), \end{cases}$$

where subscripts r and i represent reversible and irreversible traps, respectively.

Another approach based on Fick's laws is the model of hydrogen multichannel diffusion [14]. Multiple channels associated with trap sites are assumed.

The generally accepted methods of activation energies' experimental estimation is thermal desorption mass spectroscopy (TDS) [15] and its modifications [16] and experimental layouts for measuring hydrogen sorption [17]. This method generally includes a hydrogen pre-charged material, then measuring its desorption flux in vacuum or in a constant inert gas flow during a constant heating rate. The determination of activation energy is based on the famous Kissinger equation (4.1) [18].

$$\frac{\partial \ln \frac{v_T}{T_p^2}}{\partial \frac{1}{T_p}} = \frac{U}{R}, \tag{4.1}$$

where v_T is a heating rate, T_p is a peak temperature, U is an activations energy, and R is the gas constant.

It is considered that the peaks of TDS spectra are attributed to the corresponding energy [5, 10, 13, 19]. Peak temperatures are measured at few heating rates, an activation energy of hydrogen is determined as a slope of the Choo-Lee plot for each traps' group [20].

Basically, in an analysis, the hydrogen distribution in the sample is assumed to be uniform after hydrogen precharging. The simulation of the ordinary diffusion equation with one activation energy gives a desorption curve with 2 peaks at an initial non-uniform hydrogen concentration as shown in the works [15, 21, 22]. It is noted that non-uniform surface hydrogen causes a new peak to appear at low temperatures. However, the effect of the non-uniform distribution of hydrogen on TDS curves needs more clarity.

The present article is focused on the influence of explicit non-uniform hydrogen concentration on TDS. First, the diffusion equation solution is considered taking into account the non-uniform initial data in the case of 1D Cartesian coordinates. It is shown that the dependence $\ln(v_T/T_p^2)$ versus $1/T_p$ on Choo-Lee plot in the case of a non-uniform initial hydrogen distribution has a nonlinear form. Numerical calculation according to Fick's laws with the non-uniform initial conditions gives excellent agreement with the experimental data. It is shown in the example of TDS data for steel from paper [23]. The calculation of the diffusion equation is carried by the finite difference method in the case of axisymmetric cylindrical coordinates.

4.2 Dependence of Peak Temperature on Flux and Heating Rate

An ordinary diffusion equation in Cartesian coordinates with a specific piece linear initial condition is reviewed. The system of diffusion equations for a sample half with a boundary and initial condition follows:

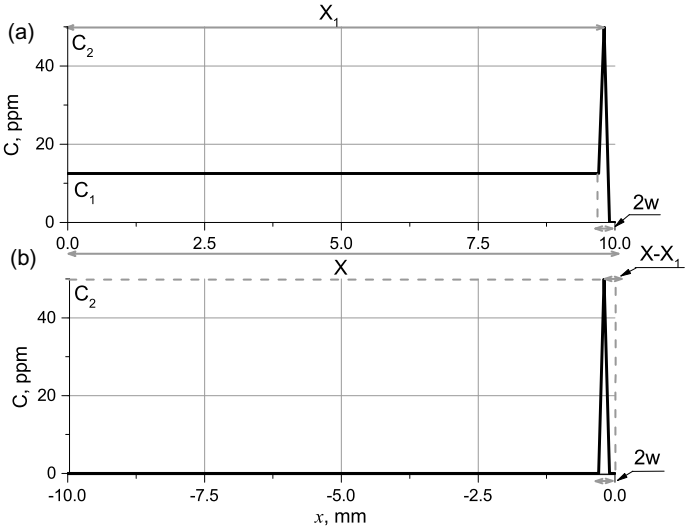

Fig. 4.1 The schematic function $C_{in}(x)$ of initial condition for the system of equations **a** (4.2) and **b** (4.5)

$$\begin{cases} \dfrac{1}{D(t)}\dfrac{\partial C}{\partial t} = \dfrac{\partial^2 C}{\partial x^2}, \\ C(t,x)|_{x=X} = 0, \\ \dfrac{\partial C(t,x)}{\partial x}|_{x=0} = 0, \\ C(0,x) = C_{in}(x), \end{cases} \tag{4.2}$$

where C is a hydrogen concentration, $D(t) = D_0 \exp\left(\frac{-U}{RT(t)}\right)$ is a diffusion coefficient, D_0 is a pre-exponential coefficient, U is an activations energy, and R is the gas constant and $T(t) = v_T t + T_0$ is a linear function of temperature dependent on time, v_T is a constant heating rate. $C_{in}(x)$ is a piecewise linear function of the initial condition, it is shown schematically on Fig. 4.1a. The initial condition corresponds to the situation, which can be as a result after hydrogen pre-charged, namely, a constant initial concentration is in the sample middle and a high hydrogen concentration is at the sample edge. Artificial saturation that is carried out in solutions leads to the fact that hydrogen accumulates at the boundary of the sample and does not pass inside. The possibility of such a hydrogen distribution in a sample after saturation is mentioned in the experimental work [23]. It is supposed in paper [21] that hydrogen gradient results from the diffusion of the adsorbate in the bulk.

Analytical solution for equation (4.2) can be written using the Fourier method. Hydrogen flux at edges is the most useful for analysis TDS, and the flow formula in the case of one-dimensional Cartesian coordinates is shown below:

$$q_H = -D(t)\frac{\partial C}{\partial x}|_{x=X} = D(t)\sum_{n=0}^{\infty} a_n T_n(t), \tag{4.3}$$

where $\lambda_n = \left(\frac{1}{2}+n\right)\frac{\pi}{X}$, $I(T) = \int_0^t \exp\left(\frac{-U}{kT(s)}\right)ds$, $T_n(t) = \exp\left(-D_0\lambda_n^2 I(t)\right)$ and coefficient a_n is given by

$$a_n = (-1)^n \frac{2\sin(w\lambda_n/2)}{w\lambda_n X}\left[(C_2 - C_1)\sin\left(\lambda_n(X_1 - \frac{w}{2})\right) - C_2\sin\left(\lambda_n(X_1 + \frac{w}{2})\right)\right].$$

The flux according to formula (4.3) has two peaks, typical profile of flux (4.3) is shown in Fig. 4.2. Figure 4.2 shows that form of flux q_H is highly dependent on heating rates v_T. The first peak can be very narrow at heating rate $v_T = 0.01$ K/min, visible as at heating rate $v_T = 0.05$ K/min, and it can be swallowed up by the second peak as at heating rate $v_T = 1$ K/min. The form flux as Fig. 4.2a can often be found in experimental data, for example [24–26].

The second peak depends on the uniform distribution of hydrogen in the sample central part and it is described by the first mode of solution (4.3), this is shown in paper [14]. The expression for the dependence of the maximum temperature on the heating rate is expressed by formula (4.4), which is a condition on the extremum of the first mode and is like the famous Kissinger formula (4.1).

$$\ln\left(\frac{v_T}{T^2}\right) = \ln\left(\frac{R}{U}D_0\lambda_0^2\right) - \frac{U}{R}\frac{1}{T}. \tag{4.4}$$

We would like to understand connection between the first peak hydrogen flux and high hydrogen concentration near-edge sample. That is, it is necessary to consider diffusion equations (4.2) with initial condition as in Fig. 4.1a with $C_1 = 0$. But we can consider a simpler task at half-infinity (4.5) with initial condition as on Fig. 4.1b, because they have a similar hydrogen flow at the edge

$$\begin{cases} \dfrac{1}{D(t)}\dfrac{\partial C}{\partial t} = \dfrac{\partial^2 C}{\partial x^2}, \\ C(t,x)|_{x=0} = 0, \\ C(0,x) = C_{in}(x), -\infty < x \le 0, \end{cases} \tag{4.5}$$

where the function $C_{in}(x)$ has a form as in Fig. 4.1b.

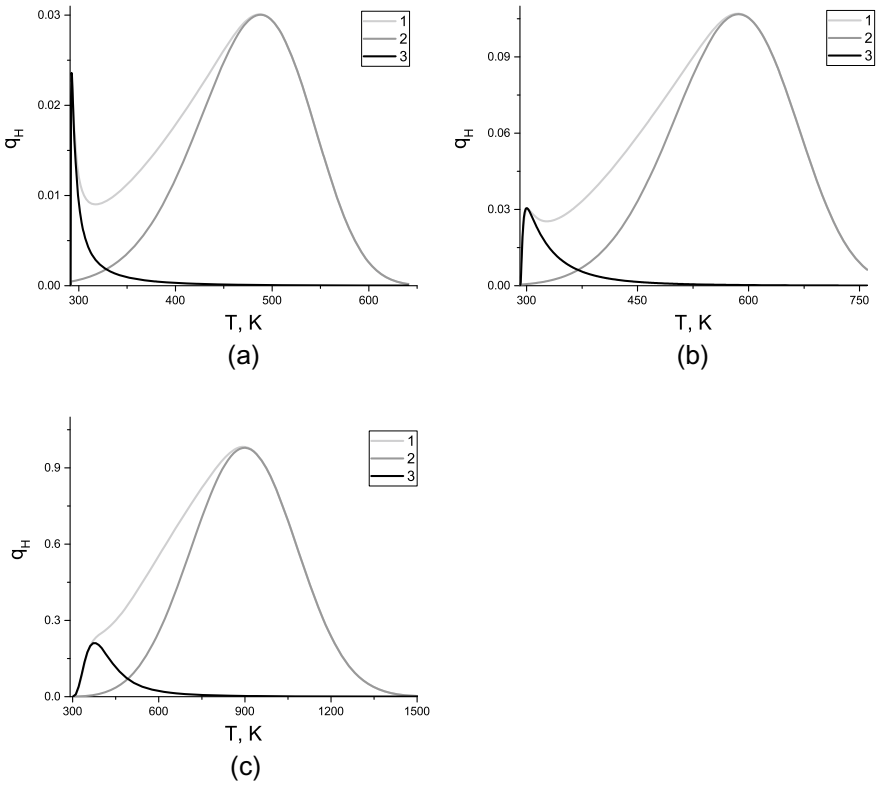

Fig. 4.2 Assessing the effect of the distribution of hydrogen in a sample on the shape of a hydrogen flux. Curve 1 corresponds to formula (4.3), curve 2 corresponds to first term of formula (4.3), and curve 3 corresponds to formula (4.6). **a** $v_T = 0.01$ K/min; **b** $v_T = 0.05$ K/min; **b** $v_T = 1$ K/min. Parameters are shown in Tables 4.1 and 4.2

Table 4.1 Material parameters value

U, kJ/mol	T_0, K	$D_0, mm^2/s$
30	291	10

Table 4.2 Geometry parameters value

X, mm	X_1, mm	w, mm	C_1/C_2
10	9.8	0.1	1/4

Solution of the system (4.5) can be written using the Fourier transform and hydrogen flux at the edge can be presented as

$$q_H = -D(t)\frac{\partial C}{\partial x}|_{x=0} = -D(t)S(t), \tag{4.6}$$

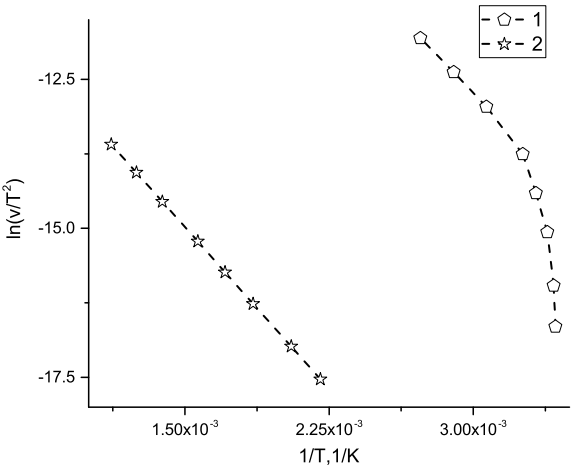

Fig. 4.3 Choo - Lee plot for parameters in Tables 4.1 and 4.2. Line 1 corresponds to Eq. (4.7) for first peak, line 2—(4.4) for second peak

where

$$S(T, v_T) = \sqrt{\frac{\pi}{2}} \int_0^\infty q C_{in}^*(q) exp(-q^2 D_0 I(t)) dq,$$

with C_{in}^* is the Fourier sine transformation of the function C_{in}. Comparison of full hydrogen flux and the first term of the original task (4.3) and hydrogen flux of the auxiliary task (4.6) are presented in Fig. 4.2. The flux of original task (4.3) and the flux of the auxiliary task (4.6) coincide at low temperatures. It can be concluded that the first peak corresponds to the desorption near-boundary hydrogen, and expression for the first peak for equations (4.2) coincides with the expression for equations (4.5). The first peak condition of flux (4.3) can be presented as (4.4).

$$\frac{1}{T^2} = \frac{R}{U} \frac{S'(t)}{S(t)}. \tag{4.7}$$

In a simple case, the flux (4.3) of the ordinary diffusion equation (4.2) with a piece linear initial condition has two peaks and dependence extreme temperatures on heating rate is nonlinear in Choo-Lee plot, see Fig. 4.3. The dependence for the second peak, which associated with the exit of bulk hydrogen, is linear in coordinates $1/T$ and $\ln\left(\frac{v_T}{T^2}\right)$. But the dependence for the first peak has two asymptotics, for "low" heating rates is a vertical line, for "higher" one is a line with slope of U/R as for the second peak and nonlinear dependence for middle heating rates.

Typically, samples are tested at several heating rates and data may lay on different sections of the line (4.4). The error of determining the energy can be huge if there is no understanding under what mode of heating these data were obtained: at low, high, or intermediate heating rates. If the experimental points correspond to a high or low heating rate, then the energy value for the first peak will coincide with the energy for the second or it will be very large. The value of energy will be questionable and

will only require further research on the data. But if the experimental points belong to intermediate heating rates or to different types of heating rates, then the energy value is arbitrary, but it is reasonable. This will allow making a wrong conclusion about a new type of trap with the corresponding energy.

We can conclude that the assumption that each hydrogen flux peak is associated with activation energy can be incorrect for some cases. Thus it is necessary to consider influence from hydrogen distribution in a sample after pre-charged. To assess the influence of the initial conditions, it is necessary to compare the experimental data and the simulation results of the corresponding equations.

4.3 Simulation and Comparison with Experimental Data

Popular forms of experimental samples are disk or cylinder. Consequently, a solution diffusion equation in axisymmetric cylindrical coordinates is needed for comparable analysis experimental and model data. The diffusion equation in axisymmetric cylindrical coordinates for half sample is shown below:

$$\begin{cases} \dfrac{1}{D(t)}\dfrac{\partial C}{\partial t} = \dfrac{\partial^2 C}{\partial z^2} + \dfrac{1}{r}\dfrac{\partial}{\partial r}\left(r\dfrac{\partial C}{\partial r}\right), \\ C(t,r,z)|_{z=X_z} = C(t,r,z)|_{r=X_r} = 0, \\ \dfrac{\partial C(t,r,z)}{\partial z}|_{z=0} = 0, \\ C(t,r,z)|_{t=0} = C_{in}(r,z), \end{cases} \tag{4.8}$$

where $2X_z$ is a sample height, X_r is a sample radius . $C_{in}(r,z)$ is a piece linear function along the r and z axes. $D(t)$ is a diffusion coefficient, which depends on time $D(t) = D_0 \exp \frac{-U}{RT(t)}$.

System (4.8) is solved numerically, using an semi-implicit finite difference scheme (4.9) with uniform grid in r and z.

$$\begin{cases} \dfrac{r_i}{D(t^{n+1/2})}\dfrac{C_{i,j}^{n+1/2} - C_{i,j}^{n}}{\Delta t/2} = \Delta_r(1/2) + \Delta_z(0), \\ \dfrac{r_i}{D(t^{n+1})}\dfrac{C_{i,j}^{n+1} - C_{i,j}^{n+1/2}}{\Delta t/2} = \Delta_r(1/2) + \Delta_z(1), \end{cases} \tag{4.9}$$

where

$$\begin{cases} \Delta_r(\alpha) = \dfrac{r_{i+1/2}\frac{C^{n+\alpha}_{i+1,j}-C^{n+\alpha}_{i,j}}{\Delta r} + r_{i-1/2}\frac{C^{n+\alpha}_{i-1,j}-C^{n+\alpha}_{i,j}}{\Delta r}}{\Delta r}, \\ \Delta_z(\alpha) = r_i \dfrac{C^{n+\alpha}_{i,j+1} - 2C^{n+\alpha}_{i,j} + C^{n+\alpha}_{i,j-1}}{\Delta z^2}, \end{cases}$$

with superscript means a point in time, for examples, $t^{n+1} = t^n + \Delta t$, $t^{n+1/2} = t^n + \Delta t/2$, subscript corresponds to a coordinate in space $C_{i,j} = C(r_i, z_j)$ is a concentration at the point (r_i, z_j) and $r_{i+1} = r_i + \Delta r$, $r_{i+1/2} = r_i + \Delta r/2$, where $0 \le i < N, 0 \le j < M$.

The calculation is carried out for half of the sample with boundary conditions

$$C_{N,j} = C_{i,M} = C_{i,1} - C_{i,0} = 0, \qquad 0 \le i < N, 0 \le j < M.$$

Our solution strategy (4.9) includes two steps: (i) in the first half of the time step, the flux in the direction of the z-axis is taken at the previous time; (ii) in the first half of the time step, the radial flux is taken at the previous moment in time. The Thomas algorithm is used to solve each equation of system (4.9). Hydrogen flux as the sum of the fluxes from the side surface and two ends is calculated as

$$q_H = 2\pi X_r D^n \sum_{i=0}^{N-1} \frac{C^n_{i+1,M} - C^n_{i,M}}{\Delta r}\Delta z + \\ + 4\pi X_r D^n \sum_{j=0}^{M-1} \frac{C^n_{N,j+1} - C^n_{N,j}}{\Delta z}\Delta r \qquad (4.10)$$

Modeling of experimental data can be provided by formulas (4.10). Experimental data are taken from work [23], ferrite-bainite steels circular samples of 20 mm diameter and 1 mm thickness were tested at 3.33, 6.66, 13.3, and 20 heating rate K/min, see Fig. 4.4.

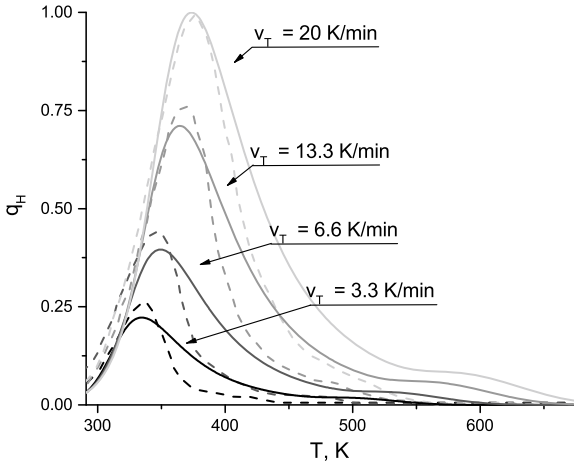

Fig. 4.4 Calculated (by the present model eq. (4.8)) and experimental curves [23] for samples at heating rate 3.33, 6.66, 13.3, 20 K/min. All curves are normalized to the flux maximum value at a temperature of 20 K/min. Parameters value are seen in Tables 4.3, 4.4

Table 4.3 Material parameters value from Ref. [23]

U, kJ/mol	T_0, K	D_0, mm^2/s
42.7	291	230

Table 4.4 Geometry parameters value from Ref. [23]. The subscripts r and z denote the coordinates r and z, respectively

X_r, mm	X_{1r}, mm	w_r, mm	X_z, mm	X_{1z}, mm	w_z, mm	$C_{1r}/C_{r2}/C_{1z}/C_{2z}$
10	9.83	0.1	0.5	0.474	0.024	1/1/1/200

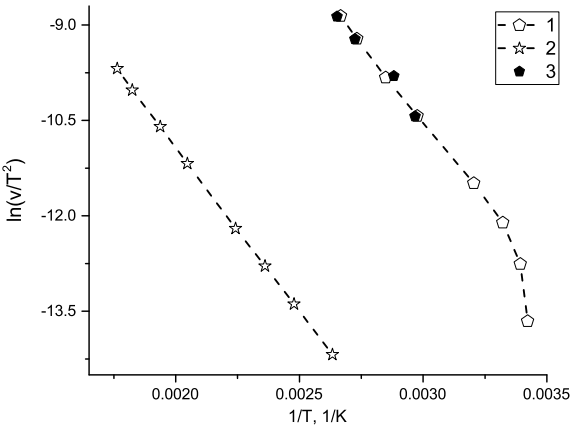

Fig. 4.5 Calculated Choo-Lee plot. Lines 1 and 2 are the numerical data (by the present model Eq. (4.8)), parameters value see in Tables 4.3, 4.4. Line 1 corresponds to equation (4.7) for first peak, line 2—(4.4) for second peak. Black circles (line 3) are experimental data from paper [23]. Additional points are shown for heating rates 0.1, 0.5, 0.5, and 1 K/min

Curves have two peaks, according to our assumption and formulas (4.4, 4.7), the slope in Choo-Lee plot for the second peak determines the activation energy U of equation (4.8). Geometry parameters and D_0 are unknown. They are selected from a fitting of the experimental curve and the curve according to formula (4.10), data for temperature rate 20 K/min is used as a nominal curve. The material and geometry parameters are given in Tables 4.3 and 4.4. A higher concentration of hydrogen at the ends at $z = X_z$ than at surface $r = X_r$ is due to the specifics of sample preparation.

The calculated and experimental profiles for each of rates have similar forms. The slight difference in the quantitative value may be due to the heterogeneity of the samples or to the necessary refinement of the model.

Figure 4.5 shows the dependence of the $\ln(v_T/T^2)$ on $1/T$. The curve corresponding to the second peak is a straight line with a slope coefficient U/R, the curve for the first peak has two asymptotics: vertical for low heating rates and asymptotics with a slope coefficient U/R for high heating rates. According to our resolution in Chap. 4.2, the experimental data [23] corresponds to "high" heating rates. But the dependence for first peaks is more complicated and can be misleading about activation energy for low heating rates than in work [23], examples 0.1, 0.25, 0.5, and 1 K/min . This confirms the importance of understanding the range of heating rates for thermal desorption analysis.

It is necessary to note that each surface gives flux, which consists of two peaks. Real samples are three-dimensional body and they have more than one surface. Consequently, the flux can have more than two peaks, which are related only to the inhomogeneous initial hydrogen distribution in the sample, ignoring the hydrogen trap. In the case under consideration, for thin circular ones, the most important flux is the flux from the surfaces $z = X_z$.

4.4 Conclusion

In this paper, we propose a model describing the effect of the initial condition of hydrogen on TDS. Analytical calculations in the case of one-dimensional Cartesian coordinates show that the edge flux of the ordinary diffusion equation with a piecewise linear initial condition has two peaks, and the Choo-Lee plot for the first peak is a nonlinear function and has two asymptotics. The first peak of the flux corresponds to edge hydrogen, and the second peak corresponds to bulk hydrogen. It highlights the importance of heating rates range for thermal desorption analysis.

Numerical modeling of experimental data shows that the curves obtained at TDS are well described using the diffusion equation and taking into account the non-uniform distribution of hydrogen in the sample. Finite difference scheme is used for solving diffusion equation in antisymmetric cylindric coordinates.

Based on the data obtained, it can be concluded that it is necessary to take into account the effect of the hydrogen distribution in the sample after pre-charged when analyzing the experimental thermal desorption curves.

Acknowledgements This study was supported by the Russian Foundation for Basic Research (project No. 18-08-00201).

References

1. Cailletet, et al.: First report of h embrittlement of metals. Compt. Rend. **58**, 327 (1864)
2. Al-Mufachi, N., Rees, N., Steinberger-Wilkens, R.: Hydrogen selective membranes: a review of palladium-based dense metal membranes. Renew. Sustain. Energy Rev. **47**, 540–551 (2015). https://doi.org/10.1016/j.rser.2015.03.026
3. Akamatsu, T., Kume, Y., Komiya, K., Yukawa, H., Morinaga, M., Yamaguchi, S.: Electrochemical method for measuring hydrogen permeability through metals. J. Alloys Compounds **393**(1–2), 302–306 (2005). https://doi.org/10.1016/j.jallcom.2004.10.007
4. Pisarev, A.A., Ogorodnikova, O.V.: Elementary processes near the interface between hydrogen gas and solid. J. Nuclear Mater. **248**, 52–59 (1997). https://doi.org/10.1016/S0022-3115(97)00201-8
5. Johnson, W.H.: II. On some remarkable changes produced in iron and steel by the action of hydrogen and acids. In: Proceedings of the Royal Society of London **23**(156–163), 168–179 (1875). https://doi.org/10.1016/0025-5416(72)90109-7

6. Louthan, M., Caskey, G., Donovan, J., Rawl, D.: Hydrogen embrittlement of metals. Mater. Sci. Eng. **10**, 357–368 (1972)
7. Bhadeshia, H.K D.H.: Prevention of hydrogen embrittlement in steels. ISIJ Int. **56**(1), 24–36 (2016). https://doi.org/10.2355/isijinternational.ISIJINT-2015-430
8. Kirchheim, R.: Hydrogen solubility and diffusivity in defective and amorphous metals. Progr. Mater. Sci. **32**(4), 261–325 (1988). https://doi.org/10.1016/0079-6425(88)90010-2
9. McNabb, A., Foster, P.: A new analysis of diffusion of hydrogen in iron and ferritic steels. Trans. Metal. Soc. AIME **227**(3), 618 (1963)
10. Oriani, R.A.: The diffusion and trapping of hydrogen in steel. Acta metallurgica **18**(1), 147–157 (1970). https://doi.org/10.1016/0001-6160(70)90078-7
11. Johnson, H.N., Quick, N.A., Kumnick, A.: Hydrogen trapping mechanisms by permeation techniques. Scr. Metall.(United States) **13**(1) (1979). https://doi.org/10.1016/0036-9748(79)90392-2
12. Leblond, J., Dubois, D.: A general mathematical description of hydrogen diffusion in steels-I. Derivation of diffusion equations from Boltzmann-type transport equations. Acta Metallurgica **31**(10), 1459–1469 (1983). https://doi.org/10.1016/0001-6160(83)90142-6
13. Turnbull, A., Carroll, M., Ferriss, D.: Analysis of hydrogen diffusion and trapping in a 13% chromium martensitic stainless steel. Acta Metallurgica **37**(7), 2039–2046 (1989). https://doi.org/10.1016/0001-6160(89)90089-8
14. Belyaev, A.K., Polyanskiy, A.M., Polyanskiy, V.A., Sommitsch, C., Yakovlev, YuA: Multichannel diffusion vs TDS model on example of energy spectra of bound hydrogen in 34CrNiMo6 steel after a typical heat treatment. Int. J. Hydrogen Energy **41**(20), 8627–8634 (2016). https://doi.org/10.1016/j.ijhydene.2016.03.198
15. Hurley, C., Martin, F., Marchetti, L., Chene, J., Blanc, C., Andrieu, E.: Numerical modeling of thermal desorption mass spectroscopy (TDS) for the study of hydrogen diffusion and trapping interactions in metals. Int. J. Hydrogen Energy **40**(8), 3402–3414 (2015). https://doi.org/10.1016/j.ijhydene.2015.01.001
16. Evard, E., Gabis, I., Yartys, V.A.: Kinetics of hydrogen evolution from MgH2: experimental studies, mechanism and modelling. Int. J. Hydrogen Energy **35**(17), 9060–9069 (2010). https://doi.org/10.1016/j.ijhydene.2010.05.092
17. Testi, M., Bartali, R., Crema, L.: Design and optimization of Isochoric Differential Apparatus (IDA) to reduce uncertainty in H2 sorption process measurements. Int. J. Hydrogen Energy **45**(18), 10775–10796 (2020). https://doi.org/10.1016/j.ijhydene.2020.01.190
18. Kissinger, H.E.: Reaction kinetics in differential thermal analysis. Anal. Chem. **29**(11), 1702–1706 (1957). https://doi.org/10.1021/ac60131a045
19. Ma, M., Liang, L., Wang, L., Wang, Y., Cheng, Y., Tang, B., Xiang, W., Xiaohua, T.: Phase transformations of titanium hydride in thermal desorption process with different heating rates. Int. J. Hydrogen Energy **40**(29), 8926–8934 (2015). https://doi.org/10.1016/j.ijhydene.2015.05.083
20. Choo, W., Lee, J.Y.: Thermal analysis of trapped hydrogen in pure iron. Metal. Trans. A **13**(1), 135–140 (1982)
21. Mavrikakis, M., Schwank, J., Gland, J.: Temperature programmed desorption spectra of systems with concentration gradients in the solid lattice. J. Phys. Chem. **100**(27), 11389–11395 (1996). https://doi.org/10.1021/jp9537623
22. Yagodzinskyy, Y., Todoshchenko, O., Papula, S., Hanninen, H.: Hydrogen solubility and diffusion in austenitic stainless steels studied with thermal desorption spectroscopy. Steel Res. Int. **82**(1), 20–25 (2011). https://doi.org/10.1002/srin.201000227
23. Escobar, D.P., Verbeken, K., Duprez, L., Verhaege, M.: Evaluation of hydrogen trapping in high strength steels by thermal desorption spectroscopy. Mater. Sci. Eng. A **551**, 50–58 (2012). https://doi.org/10.1016/j.msea.2012.04.078
24. Takashima, K., Han, R., Yokoyama, K., Funakawa, Y.: Hydrogen Embrittlement induced by hydrogen charging during deformation of ultra-high strength steel sheet consisting of ferrite and nanometer-sized precipitates. ISIJ Int. **59**(12), 2327–2333 (2019). https://doi.org/10.2355/isijinternational.ISIJINT-2019-219

25. Fernandez, J., Cuevas, F., Sanchez, C.: Simultaneous differential scanning calorimetry and thermal desorption spectroscopy measurements for the study of the decomposition of metal hydrides. J. Alloys Compounds **298**(1–2), 244–253 (2000). https://doi.org/10.1016/S0925-8388(99)00620-9
26. Liu, Y., Wang, M., Liu, G.: Hydrogen trapping in high strength martensitic steel after austenitized at different temperatures. Int. J. Hydrogen Energy **38**(33), 14364–14368 (2013). https://doi.org/10.1016/j.ijhydene.2013.08.121